Characterisation of Mitochondria-associated ER membranes in the enteric nervous system under physiological and pathological conditions

Giada Delfino, Jean Baptiste Briand, Thibauld Oullier, Léa Nienkemper, Jenny Greig, Joëlle Véziers, Michel Neunlist, Pascal Derkinderen, Sebastien Paillusson

Characterisation of Mitochondria-associated ER membranes in the enteric nervous system under physiological and pathological conditions

Giada Delfino[1], Jean Baptiste Briand[1], Thibauld Oullier[1], Léa Nienkemper[1], Jenny Greig[2], Joëlle Véziers[3], Michel Neunlist[1], Pascal Derkinderen[1] and Sébastien Paillusson[1]*

[1] Nantes Université, INSERM, CHU Nantes, The Enteric Nervous System in Gut and Brain Disorders, Nantes, France.

[2] INSERM, Centre de Recherche en Transplantation et Immunologie, UMR 1064, ITUN, Nantes, France.

[3] Nantes Université, Oniris, Univ Angers, INSERM, Regenerative Medicine and Skeleton, RMeS, UMR 1229, F-44000 Nantes, France.

* To whom correspondence should be addressed: Sébastien Paillusson (email sebastien.paillusson@univ-nantes.fr)

Keywords: enteric nervous system, mitochondria-associated ER membranes, Parkinson's disease, Alzheimer's disease, ageing

Abstract

Alterations in endoplasmic reticulum-mitochondria associations and in mitochondria-associated ER membrane (MAM) behaviour have been reported in the brain in several neurodegenerative diseases. Despite the emerging role of the gut-brain axis in neurodegenerative disorders, the biology of MAM in the enteric nervous system (ENS) has not previously been studied. Therefore, we set out to characterise the MAM in the distal colon of wild type C57BL/6J mice and in senescence accelerated mouse prone 8 (SAMP8), a mouse model of age-related neurodegeneration. We showed for the first time that MAM are widely present in enteric neurons and that their association is altered in SAMP8 mice. We then examined the functions of MAM in a primary culture model of enteric neurons and showed that calcium homeostasis was altered in SAMP8 mice when compared to control animals. These findings provide the first detailed characterisation of MAM in the ENS under physiological conditions and during age-associated neurodegeneration. Further investigation of MAM modifications in the ENS in disease may provide valuable information about the possible role of enteric MAM in neurodegenerative diseases.

New and Noteworthy

Our work shows for the first time the presence of contacts between ER and mitochondria in the enteric neurons and that the dynamic of these contacts is affected in these cells from an age-related neurodegeneration mouse model. It provides new insights into the potential role of enteric MAM in neurodegenerative disorders.

Introduction

The interaction between endoplasmic reticulum (ER) and mitochondria is a key regulator of many neuronal functions including calcium and mitochondrial homeostasis, phospholipid synthesis, autophagy and synaptic activity amongst others (1). These contacts, termed Mitochondria-associated ER membranes or MAM, are physically tethered by protein bridges that finely tune ER and mitochondria associations (2, 3). Over the last decade, alteration in both MAM dynamics and signalling have been consistently associated with age-related neurodegenerative disorders such as Parkinson's disease (PD) and Alzheimer's disease (AD), and damage to neurons in these disorders often overlaps with cellular functions regulated by ER-mitochondria contacts and MAM signalling (1, 4).

An increasing number of studies suggest that the gut and more generally speaking the gut-brain axis has a significant impact on neurodegeneration as already described in PD (5), AD [6], and age-related neurodegeneration (6). The enteric nervous system (ENS), which is embedded within the gastrointestinal (GI) tract and regulates major GI functions, is one of the key components of the gut-brain axis (7). Compared to other components of the peripheral nervous system, the ENS shows some unique features that closely resemble the central nervous system (CNS) and is therefore sometimes referred to as 'the brain-in-the-gut' (8). This close homology between the CNS and ENS suggests that a disease process affecting the CNS could also involve its enteric counterpart. Despite the relative wealth of research on the MAM in the CNS, no data are available about the MAMs in the ENS, and this is the focus of the current study.

Here, we first characterised the MAM in the colon of wild-type (WT) mice and examined the same MAM characteristics in a mouse model of age-related

neurodegeneration (senescence accelerated mouse prone 8, SAMP8) in comparison to their control littermates (senescent accelerated mice resistant 1, SAMR1). We first showed that MAM are widely present in enteric neurons and that they are altered in the enteric neurons from SAMP8 mice. We then examined the functions and structure of MAM in a primary culture model of enteric neurons and showed that calcium homeostasis was altered in SAMP8 mice when compared to control animals. These findings provide the first detailed characterisation of MAM in the ENS under physiological conditions and in a mouse model of age-associated neurodegeneration. Further investigation of MAM modifications in the ENS in disease may provide valuable information about the role of enteric MAMs in neurodegenerative diseases.

Materials and methods

Animals

3-month-old C57BL/6J mice were obtained from Janvier Labs (Le Genest Saint-Isle, France) and immediately sacrificed for colonic tissue collection. SAMP8 and SAMR1 mice were originally obtained from ENVIGO (Gannat, France), and colonies were bred in our animal facility. Four mice were housed per cage and maintained under 12 h light/dark cycle with water and food *ad libitum*. All procedures were conducted in accordance with the guidelines for animal care and approved by the local ethic committee (APAFIS #31937). For our experiments, SAMP8 and SAMR1 mice were studied at the age of 8 months with a ratio of 50% male and female.

Primary cultures of enteric neurons

Mouse enteric neuron enriched primary cultures were adapted from Caillaud et al. 2022 (9). Briefly, intestines from embryonic day 14 (E14) mouse embryos were

isolated and dissected individually in Hanks buffered Salt solution (HBSS). Each intestine was chopped into small pieces (explants) and placed in a 24 well plate precoated with 1.2% collagen I (Ref. 354236, Corning) and cultured in enteric glia conditioned medium (9) supplemented with glial derived neurotrophic factor (GDNF) (Ref. 5126GF/CF, R&D Systems) 50 ng/mL for 1 week.

After 1 week, the explants were removed and the cells that spread over the wells were enzymatically dissociated with 300 µL of accutase (Ref. 07920, Stem Cells Technology) per well for 5 min. The enzymatic reaction was then neutralised by Dulbecco's Modified Eagle's Medium (DMEM)-F-12 (5 mL per well) (Ref. 31330-038, Gibco) supplemented with 10% foetal bovine serum (FBS) (Eurobio). Cells were then spun at 350 g for 5 min at room temperature (RT). The supernatant was then removed, and the cells were resuspended in enteric glia conditioned medium supplemented with 50 ng/mL GDNF and plated on 10 mm glass coverslips (Dutcher) or an Ibidi 8 well µ-slide (Ref. 80826, Ibidi) precoated with poly-L-lysine (Ref. P5899, Sigma) 0.1 mg/mL. After 24h, cytosine ß-D-arabinofuranoside hydrochloride (AraC) (5 µM/well) was added to reduce the quantity of enteric glia and muscle cells. Cultures were grown for 15 days in a humidified incubator set to 5% CO_2 at 37°C.

Behavioural tests

Animals were placed in the experimental room for acclimatization 1h before the start of the behavioural tests. The experimental room temperature was 23°C and the light was 40 lux. All behavioural experiments have been performed at 9 o'clock in the morning for circadian rhythm consistency. A 50% male/female ratio was used for these tests. Data analysis was performed blinded.

Open Field

Mice were individually placed in a square plexiglass box (50 cm x 50 cm) and allowed to move freely for 10 min while being recorded by an overhead camera. The locomotory activity was measured by an automated video tracking system (LabVIEW) for the following parameters: total distance travelled, and time spent in a pre-defined area.

Elevated plus maze

Mice were individually placed in the centre of an elevated plus maze which had two open and two closed arms. Animals were allowed to move freely for 5 min while being recorded by an overhead camera. The following parameters were measured by an automated video tracking system (LabVIEW): the total distance travelled, and the time spent in the open arms.

Gastrointestinal tests

Total transit time and pellet output were measured as described previously (10) using the carmine red method. Carmine red (60 mg/mL) suspended in 0.5% (v/v) carboxymethylcellulose was administered by gavage. The volume of carmine red solution for each animal was calculated based on animal weight (0.3 mg/g), pellet output was monitored, and the total transit time was calculated as the time interval between gavage and the first red pellet. Colonic transit time was measured with the pellet output test. Mice were individually placed in clean, clear cages without food and water for 2 h. Pellets were collected in a tube, counted, and weighed to obtain the fresh stool weight, then dried for 48 h at 65°C and reweighed to obtain the dry stools weight. The percentage of water content was calculated as the difference

between wet and dry stool weight. All gastrointestinal experiments have been performed at 9 o'clock in the morning for circadian rhythm consistency. A 50% male/female ratio was used for these tests. Data analysis was performed blinded.

Electron microscopy

Mice were anaesthetised by isoflurane and transcardially perfused with freshly prepared 4% (v/v) formaldehyde in phosphate buffered saline (PBS) at pH 7.4. Tissue from distal colon was isolated and post fixed for 24 h in 2.5% (v/v) glutaraldehyde in 0.1 M cacodylate buffer (Ref. 41920134-3, Bioworld) at pH 7, then washed in 0.1 M cacodylate buffer and post fixed for 1 h in 1% (w/v) osmium tetroxide (Ref. AGR1015, Agar Scientific) and 1.5% (w/v) ferricyanide (Ref. P3289, Sigma) in 0.1 M cacodylate buffer (11). Tissues were then dehydrated and embedded in epoxy resin (Agar Scientific Ltd, Stansted UK), 80 nm thin slides were cut on a Leica EMUC7 ultramicrotome, placed on a 200 mesh EM (Agar Scientific Ltd, Stansted UK) grid and stained in Uranyless/3% lead citrate according to Reynolds method (Ref. 11300, Delta Microscopies) for 5 min. Low magnification images were acquired with backscattered electrons at 20 kV with a Zeiss Gemini SEM300 (Oberkochen, Germany). High magnification images were acquired with a S/TEM Themis Z G3 (Thermo Fisher Scientific)

Antibodies

Primary antibodies: mouse anti- protein gene product 9.5 (PGP9.5) (Ref. MA1-83428, Invitrogen*, Dilution: 1/200 IF and 1/500 WB*); goat anti-HuD (Ref. sc5977., Santa Cruz, *Dilution: 1/200 IF*); human anti-HuD (Gift from CHU Nantes *Dilution: 1/500 IF);* mouse anti-VAPB (Ref. 66191-1, Proteintech, *Dilution: 1/500 WB*); rabbit anti-

PTPIP51 (Ref. HPA009975, Atlas Antibodies, *Dilution:1/500 WB*); mouse anti-mitofusin 2 (MFN2) (Ref.sc-100560, Santa Cruz, *Dilution: 1/1000 WB*); mouse anti-sigma-1 Receptor (Ref. sc-137075, Santa Cruz, *Dilution: 1/1000 WB*); mouse anti-actin beta (Ref. A5441-2ML, Sigma-Aldrich, *Dilution:1/5000 WB*).

Secondary antibodies: for IHC the following secondary antibodies were used: biotinylated anti-goat secondary antibody (Ref. BA-9500, VECTOR, dilution:1/200) and IHC the following secondary antibodies were used: anti-human Alexa Fluor 488 (Ref. H10120, Life. *Dilution: 1/500*); anti-mouse Alexa Fluor 647 (Ref. A31571, Invitrogen. *Dilution: 1/400*);

For western blotting, the following secondary antibodies were used: horseradish peroxidase-conjugated anti-mouse (Ref. A9044, Sigma-Aldrich. *Dilution: 1/5000*); horseradish peroxidase-conjugated anti-rabbit (Ref. 31460, Thermo Fisher. *Dilution: 1/5000*).

Kluver – Barrera staining

Mouse brains were quickly dissected and immediately emerged in freshly prepared 4% (v/v) formaldehyde in PBS for 48 h before being embedded in paraffin. 5 µm sagittal sections were then prepared on a microtome and processed as follows: sections were immersed in successive washes of xylene (2 x 5 min), absolute ethanol (2 x 5 min), 70% (v/v) ethanol (1 x 5 min) and purified H_2O (2 x 5 min). Slides were stained according to Klüver and Barrera (12) and were then mounted in Entellan anhydrous mounting medium (Ref. 107960, Sigma-Aldrich). Images were acquired on an OLYMPUS BX51 microscope with a 40x objective.

Proximity ligation assay (PLA)

Mice were anaesthetized by isoflurane and transcardially perfused with freshly prepared 4% (v/v) formaldehyde in PBS at pH 7.4. Tissue from the distal colon was isolated and post fixed for 24 h in 4% formaldehyde in PBS, pH 7.4. Then, 3 µm sagittal sections were prepared on a microtome and processed as follows. Sections were immersed in successive washes of xylene (2 x 5 min), absolute ethanol (2 x 5 min), 70% (v/v) ethanol (1 x 5 min) and purified H_2O (2 x 5 min). Antigen retrieval was performed with tris-EDTA buffer with 0.05% Tween-20 for 8 min at 95°C, then, sections were washed in PBS with 0.2% Tween-20 for 4 h.

In situ PLA were performed with the Duolink® PLA Brightfield (Ref. DUO92012, Sigma-Aldrich) according to the manufacturer's instructions with some modification. Washing steps were performed in 1X wash buffer A (3 x 5 min). Slides were incubated with hydrogen peroxide solution for 15 min at RT, then washed and incubated in blocking buffer for 60 min at 37°C. Following this, slides were washed and incubated with primaries antibodies (anti-PTPIP51 (Ref. HPA009975, Atlas Antibodies *dilution: 1/200*) and anti-VAPB (Ref. 66191-1 Proteintech, *dilution: 1/200*)) overnight at RT. The next day, slides were washed and incubated with the PLUS and MINUS probes, diluted 1/20 in antibody diluent for 1 h at 37°C in a preheated humidity chamber. Slides were washed and incubated with ligase diluted at 1/40 in 1X ligation buffer for 30 min at 37°C, followed by washing steps and incubation with polymerase diluted at 1/80 in 1X amplification buffer for 100 min at 37°C. Slides were then washed and incubated in detection brightfield solution diluted 1/5 in purified water for 60 min at RT. Finally, slides were incubated in substrate solution for brightfield signal detection.

Slides were then washed in PBS-0.2% Tween-20 (3 x 5 min) and incubated overnight at RT with primary antibody goat anti-HuD (Ref. sc5977, Santa Cruz, dilution: 1/200). They were then washed and incubated in a biotinylated anti-goat secondary antibody (Ref. BA-9500, VECTOR, dilution:1/200). Signal detection was performed using Vector® VIP Substrate Kit (Ref. 705-605-147, Jackson Immuno Research) as per the manufacturer's instructions.

Slides were mounted in Entellan anhydrous mounting medium (Ref. 107960, Sigma-Aldrich). Images were acquired on an OLYMPUS BX51 microscope with a 40x objective.

Enteric neuronal count

PGP9.5 immunoreactive cells were quantified on whole mount sections (4 fields of 1,52 mm^2 per sample), with identical exposure and illumination settings on the microscope (Axio Observer, Zeiss). Then the number of PGP9.5 positive cells were reported to the surface area (mm^2). HuD count was performed on 3 µM paraffin sections (as described in the PLA section) and the number of HuD positive cells were expressed by the total surface area (mm^2).

Western blot analysis

Tissues or cells were lysed for immunoblotting in RIPA Lysis buffer 1X (Ref. 20-188, Merck Millipore) containing 0.1% phosphatases inhibitors (P0044-5ML, Sigma, Ref.), 0.1% proteases inhibitor (Ref. 66373700, Roche diagnostic,) and 0.1% sodium orthovanadate (Ref. 6508, Sigma). Protein quantification was performed using a bicinchoninic acid assay (BCA). Samples were prepared at a concentration of 1 µg/µL or 0.5 µg/µL for electrophoresis.

Proteins were denatured by heat at 95°C for 5min, then separated in NuPAGE Bis-Tris 4-12% (Ref. NP0322BOX, Invitrogen) polyacrylamide gels and transferred to nitrocellulose membrane using iBlot transfer stack (Ref. IB33002, Invitrogen), in an iBlot Western Blot transfer system (Invitrogen, France). Membranes were then blocked by incubation in TBS 1X-0.1% Tween-20 and supplemented with 5% dry milk, pH 7.5 for 1h and incubated with primary antibodies diluted in blocking solution overnight at 4°C. Subsequent wash steps were performed in TBS 1X-0.1%Tween 20 (v/v) and membranes were incubated with horseradish peroxidase-conjugated anti-mouse or anti-rabbit antibodies. Immunoblots were developed using Clarity Western ECL substrate (Ref. #1705060, Biorad) or Super Signal West Femto Maximum Sensitivity substrate (Ref. 34094, Invitrogen) according to the manufacturer's instructions. Images were acquired with a ChemiDoc Imaging System (BioRad) and signals were quantified using ImageJ software.

Mitochondrial calcium imaging

SAMP8 and SAMR1 enteric neuron enriched primary cultures were loaded with 1 µM Rhod2-AM dye (Ref. ab142780, Abcam) in live cell imaging solution (Ref. A1429IDJ, Invitrogen) containing 0.004% Pluronic F-127 (Ref. P3000MP, Invitrogen) for 30 min at 37°C. Cells were washed in live cell imaging solution prior to image acquisition. Oxotremorine-M (Ref. 63939-65-1, Santa Cruz,) was added during the image acquisition (after ~20s), at a final concentration of 100 µM.

Timelapse images were acquired during 90s (1s intervals) with a Leica DMi8 video microscope objective 20x at 37°C. Ca^{2+} levels were calculated as the relative Rhod2 fluorescence compared to the fluorescence baseline (F/F_0).

To assess the specificity of OxoM on ER calcium release, primary neurons were loaded with 3 µM of a photoactivable form of IP3. After obtaining basal fluorescence levels, UV flash photolysis ensures the rapid release of active IP3. The results showed that the pattern of calcium traces induced by caged IP3 was comparable to the one obtained with OxoM (fig. S3B).

Statistical analysis

All data shown are mean ± standard error of the mean (SEM). Statistical analyses were conducted using GraphPad software version 9. (San Diego California, USA). For comparisons of means between two groups, Unpaired Student-t-test or Mann Whitney tests were employed. ER-mitochondria distribution comparison was assessed by a 2 way-ANOVA test. Differences were deemed statistically significant when $p < 0.05$.

Results

Enteric neurons contain ER-mitochondria associations

In order to determine if ER-mitochondria contacts are present in enteric neurons under physiological conditions, colonic samples from 3-month-old male C57BL/6J mice were analysed by electron microscopy (EM). We first identified enteric neurons of the myenteric plexus at low magnification that were embedded between the circular and longitudinal muscle (fig. 1A), then we observed interactions between ER and mitochondria that ranged from 10 to 30 nm (13) occurring in enteric neurons (fig. 1B and C). ER-mitochondria contacts were mostly found in the soma, around the nucleus where most of the ER is located, but some interactions are sporadically present at synapses. Such observations have already been made in hippocampal

primary neurons (14). We then looked at higher magnification into ER-mitochondria contacts (fig. 1D, and E), where we observed some filamentous structures bridging the ER and the mitochondria together and which resemble the molecular tethers that have already been described elsewhere (4) (fig. 1F). Quantification of the total mitochondria surface in contact with ER membrane showed that most of mitochondria had less than 20% contact (fig. 1D) with a length below 200 nm (fig. 1E). In cells, MAM functions are finely tuned by the distance between ER and mitochondria [4] and we found that the distance between the majority of ER membrane and mitochondria contacts ranged most frequently between 10 and 20 nm (fig. 1F).

The inter-organelle space between ER and mitochondria is calibrated by tethering proteins that physically maintain the two organelles together (3). One well-characterised tether involves an interaction between the integral ER protein, vesicle-associated membrane protein-associated protein B (VAPB) and the outer mitochondrial membrane protein, protein tyrosine phosphatase interacting protein-51 (PTPIP51) (13, 15) . This VAPB-PTPIP51 tether controls a number of ER-mitochondria regulated functions such as mitochondrial ATP production (11, 13) and autophagy (16, 17). Using Western blot (WB) analysis, we showed that these two key tethering proteins were present in mice colonic lysates (fig. 1G). We also showed that mitofusin 2 (MFN2) (18), another tethering protein and the ER-resident protein Sigma-1 receptor (Sig1R), a regulator of MAM association and homeostasis (19), were also expressed in the distal colon of 3-month-old C57BL/6J mice (fig. 1G). To further refine this analysis, *in situ* proximity ligation assay (PLA) was used to examine the localization of VAPB-PTPIP51 association (20, 21) in the mice ENS. To demonstrate the specificity of PLA, we first performed control experiments in which

primary VAPB and/or PTPIP51 antibodies were omitted and as expected, no signal was observed (fig. 1H, I and J). In contrast, multiple dots were observed when the two antibodies were used in combination both in enteric neurons (stained with Hu-antibodies) and in non-neuronal cells (fig. 1K).

When taken together, these results show that enteric neurons contain ER-mitochondria associations. In addition, our work indicates that two of the main MAM tethering proteins, VAPB and PTPIP51 are expressed by enteric neurons.

Senescent Accelerated Mouse-Prone 8 (SAMP8) exhibit central and enteric functional defects at 8 months of age

In order to study MAM in the gut under pathological conditions, we examined the possible alterations of enteric MAM in a mouse model of ageing and age-related neurodegeneration, namely the Senescence Accelerated Mouse-Prone 8 (SAMP8) model (22, 23) . We chose this model for several reasons: (i) first, and most importantly, it is a non-transgenic, naturally occurring mouse line that displays a phenotype of accelerated ageing (ii) it gradually develops CNS neurodegeneration together with behavioural disorders (iii) a preliminary report showed that these mice exhibit morphological (AD-related protein deposition) and functional (impaired colonic excitatory neurotransmission) changes in their GI tract starting at 6 months of age (24). Before using this model for the characterization of enteric MAMs in pathological conditions, we set out to verify if, in our hands, these mice displayed CNS and GI dysfunction. In line with previous findings (25), we first showed that 8-month-old animals had a significant neuronal loss in the CA3 subregion of the hippocampus compared to the normal aging SAMR1 control mice as evaluated by immunohistochemistry (Klüver-Barrera Staining) (fig. 2A) and by WB (fig. 2B, C). We

then evaluated whether this neuronal loss was associated with behavioural changes. In the open field test (fig. 2D, cartoon), SAMP8 mice covered a significantly longer distance (fig. 2D left bar graph) and spent more time in the centre compared to control mice (fig. 2D right bar graph). In the elevated plus maze (fig. 2E cartoon), SAMP8 mice travelled significantly further (fig. 2E left bar graph) and spent more time in the opened arm than control mice (fig. 2E right bar graph). In line with previous findings (25, 26), our results show hyperactivity and reduction of the fear behavior in both male and female SAMP8 mice (fig. S2) compared to controls.

Regarding the GI tract, SAMP8 mice had a decrease in immunoreactivity for PGP9.5 (fig. 3A, B) and a significant reduction in Hu positive cells (fig. 3C) in the distal colon when compared to SAMR1 mice, demonstrating neuronal loss in the distal colon of the SAMP8 mice. From a functional point of view, SAMP8 mice exhibited a shorter total gut length (fig. 3D left bar graph) together with a longer total transit time compared to control mice (fig. 3D right bar graph) which tend to occur mostly in males (fig. S2). In addition, SAMP8 mice produced less stools over a 2h period overall (fig. 3E left panel), which is more prominent in males when the data were segregated by sex (fig. S2) and their fresh stool weight was significantly lighter compared to the SAMR1 mice (fig. 3E right panel) but was this time more prominent in females (fig. S2). These data, which confirmed earlier findings showing that SAMP8 mice exhibit both CNS and GI defects (24–26), indicate that this mouse model can be reliably used to study the effects of age-related neurodegeneration on ER–mitochondria associations in enteric neurons.

ER-mitochondria associations are altered in the enteric neurons during age-related neurodegeneration

In order to study the effects of age-related neurodegeneration on the interactions between ER and mitochondria in enteric neurons, colonic samples from 8-month-old SAMP8 mice were analysed by EM and compared to age-matched SAMR1 control mice. In order to overcome the possible confounding role of mitochondria size on the analysis of ER-mitochondria associations, ER–mitochondria associations were quantified by analysing the total mitochondrial surface that was closely apposed (≤30 nm) to ER in colonic enteric neurons as previously described (11, 13). In doing so, the mitochondria size does not affect the results even in the case of a change in mitochondrial size. When compared to control mice, the average percentage of mitochondrial surface in contact with ER membranes and the average contact length between the two organelles were respectively significantly higher (fig. 4A and B) and longer (fig. 4A and C) in SAMP 8 mice. In contrast, no difference was observed between the two groups of animals when the ER-mitochondria distance was quantified (fig. 4D). We also found a significant reduction in mitochondrial surface area in SAMP8 mice compared to controls (fig. 4E). We have also represented the individual distribution of the mitochondrial surface apposed to ER (fig. 4F), the distribution of ER-mitochondria contacts length (fig. 4G) and the distance between ER and mitochondria (fig. 4H) in order to track a more specific change in ER-mitochondria associations between SAMR1 and SAMP8 mice.

Besides enteric neurons, intestinal muscles are the other key effectors of intestinal motility, and we therefore quantified the ER-mitochondria contacts in smooth muscle cells from the longitudinal muscle of the GI tract. No statistical difference was found between the two groups regarding ER-mitochondria association (fig.S1A), average contact length (fig.S1B), distance between the two organelles (fig.S1C), mitochondrial surface (fig.S1D) or mitochondrial surface area (fig. S1E).

MAM signalling is altered in the enteric neurons in age-related neurodegeneration

The vast majority of MAM cellular functions can only be studied in cell culture models and not in adult tissue. This is especially the case for studying the exchange of calcium between the ER and mitochondria, a key function in cellular homeostasis. Indeed, these calcium exchanges between both organelles need to be tightly regulated as too little calcium in the mitochondria impacts the production of ATP by oxidative phosphorylation (11, 27), whereas calcium overload in the mitochondria triggers cellular apoptosis (28). The brain is not the only source from which neurons can be cultured and there are now established protocols for the isolation of enteric neurons from rodents (9). We therefore took advantage of this approach to study the calcium exchange between ER and mitochondria in primary enteric neurons from SAMR1 and SAMP8 mice. We first showed that the MAM tethers including PTPIP51, VAPB and Mitofusin 2 were expressed in these primary cultures of enteric neurons (fig 5A) and that the expression levels of these proteins were comparable between SAMP8 and SAMR1 primary enteric neurons (fig 5A, B, C and D). Also, we found no statical differences in either enteric neurons or glial cell numbers between SAMR1 and SAMP8 primary cultures (fig. S3A), indicating no neuronal death or reactive glia at this stage. To study mitochondrial calcium homeostasis, the release of ER-stored calcium was induced by the muscarinic receptor activator oxotremorine M (OxoM) and the calcium uptake by mitochondria was monitored using the rhodamine 2 (Rhod-2) calcium sensor. We found that the mitochondrial calcium uptake in the SAMP8 primary enteric neurons was significantly higher (fig.5E, F Fmax/F0= 1,55 ±0,031) compared to SAMR1 primary enteric neurons (fig.5E, F Fmax/F0= 1,27 ±0,012).

These results show that in SAMP8 mice, calcium exchange from the ER to the mitochondria is facilitated and therefore suggests that more ER-mitochondria contacts occur in SAMP8 primary neurons compared to the SAMR1 control neurons, since the calcium entry from the ER to the mitochondria is facilitated through the IP3R-VDAC complex in MAM (2). Our findings are in line with the literature, where an increase in MAM is typically associated with more calcium uptake from the mitochondria whereas less contacts have been reported to reduce the mitochondrial uptake (see (29) for a review). Such findings have been consistently reported in many cell types and especially central (11, 14, 30, 31) and motor neurons (13, 20), and confirmed our previous results obtained by EM in colonic neurons (fig.4).

Discussion

Despite the relative wealth of studies on MAMs in neurons of the brain, nothing is known about MAMs in neurons from the gut, which is the second largest neurological organ in the human body (32). Here, we have identified for the first time the presence of ER-mitochondria contacts in the enteric neurons and using electronic microscopy, we provided a detailed characterisation of these interactions. We first showed that mitochondria naturally interact with ER membranes to form MAMs in enteric neurons of the myenteric plexus of young adult C57BL/6J mice and found that ~14% of the total surface of the mitochondria was in contact with ER membranes. We also characterised the distribution of these contacts in length, space between the organelles and the mitochondrial surface occupied by ER, showing the flexibility of MAM dynamics in enteric neurons. We found that key MAM proteins were expressed in the gut and that tethers including VAPB and PTPIP51 were present and actively interacting in enteric neurons. Overall, these results are in line with those already obtained in rodent CNS neurons, including primary cortical neurons (33) and spinal

cord motor neuron (20). Interestingly, cortical and motor neurons rely substantially on MAM signalling to function properly, and as such, disruption of ER-mitochondria contacts has been shown to impact several key functions that are damaged in age-related neurological disorders (for a review see (1)). Therefore, this suggests that alterations in MAM signalling in enteric neurons could lead to detrimental effects in the GI tract.

These observations prompted us to study the ER-mitochondria associations in enteric neurons in a pathological context. We chose to use SAMP8 mice, a non-transgenic model of age-related neurodegeneration that displays both CNS and GI dysfunctions associated with Aß protein deposition in the brain (24, 34, 35), similar to that observed in AD (36–38). From a digestive point of view, our results showed an increased transit time together with fewer and dryer fecal pellets in SAMP8 compared to control animals, two features that reflect constipation, a clinical sign frequently found in AD (39) or PD patients (40). Slow transit constipation is characterised by a reduced colonic motility, which is regulated by two major actors, the ENS and smooth muscle layers: the ENS senses its environment and generates activatory and inhibitory signals to different layers of the intestinal smooth muscle to produce contractions and relaxations of the intestinal wall, essential to convey the luminal content of the gut (7). Here we found that SAMP8 enteric neurons had more ER-mitochondria contacts compared to control mice which was associated with reduction of both PGP9.5 and HuD immunoreactivity, a classical sign of enteric neuronal loss, whereas no difference in ER-mitochondria contacts was observed when longitudinal smooth muscle cells were analysed.

We also showed that in SAMP8 mice, damage to MAM signalling occurs very early on since we have reported an increase in ER-mitochondria contacts was accompanied with harmful MAM dysfunction, causing mitochondrial calcium overload in primary enteric neurons. However, we did not find any neuronal loss in our SAMP8 primary neurons (fig. S3A). These findings suggest that damage to MAM is an early feature in SAMP8 mice and could contribute towards an enteric neuronal loss in the latter adulthood, which could be responsible for digestive dysfunctions. Several aspects of the SAMP8 biology could explain an early defect in MAM. Firstly, the existence of one point mutation (41) and a mutation in the 3'UTR (42) on the APP gene could generate higher levels of APP from the embryonic stage. Several studies have reported that APP (43) is localised at the MAM and its overexpression triggers an increase in MAM associations (43–45). Some genomic studies have also identified several mutations on mitochondrial genes that could therefore contribute to early abnormalities in SAMP8 embryonic neurons (46).

When taken as a whole, our findings suggest that the slow transit constipation observed in SAMP8 mice is due to neuronal dysfunction leading to a loss in the enteric neurons rather than a functional defect in smooth muscle cells. They are in line with a recent study, which showed that, in comparison to control animals, 6-month-old SAMP8 mice had a significant decrease in stool frequency and impaired *in vitro* colonic contraction (24). More broadly, these results open new perspectives for the understanding and the treatment of chronic constipation, two aspects that remain controversial and challenging (47). There is now mounting evidence to suggest that slow transit constipation is not a functional disorder but instead an enteric neuropathy (48), with numerous studies showing that severely constipated patients exhibit abnormal features of the ENS, such as changes in the neurochemical coding (49),

myenteric plexus hypoganglionosis (50) and neuronal loss. It is therefore tempting to speculate that these ENS abnormalities may be associated with MAM morphological changes and dysfunction and that restoring MAM function in the enteric neurons might be considered as a therapeutic option for slow transit constipation. In this setting, a first critical step would be to perform an in-depth characterisation of the MAM in the myenteric plexus of severely constipated subjects.

From an anatomical point of view, the structure and the organisation of the ENS stand out from other peripheral nervous systems as they show unique features that closely resemble the CNS architecture (32): (i) the ENS displays a broad range of functionally distinct neurons along with a rich variety of neurotransmitters and messengers responsible for enteric neurotransmission (51) (ii) the morphology and characteristics of enteric ganglia is more similar to the CNS when compared to other peripheral nervous systems; (iii) like the CNS, the ENS can also be impaired by many congenital and acquired disorders, known as enteric neuropathies (52). These similarities between the ENS and CNS suggest that a disease process affecting the CNS, especially a neurodegenerative disorder, could also involve its enteric counterpart. Such a parallel involvement of the gut and the brain has already been well described for PD (see (53) for a review) and emerging findings suggest that it may also be the case in AD (54). In support of this, the increase in ER-mitochondria associations along with the alterations of MAM signalling that we are currently reporting in the gut of SAMP8 mice mirror the cellular alterations found in cortical and hippocampal neurons, two main structures affected by the disease found in many AD mice models (55–58).

From a mechanistic point of view, several studies have now reported that SAMP8 mice express higher levels of amyloid precursor protein (APP) (24, 26, 59), whose sequential cleavage generates Aß peptide. Interestingly, APP has been shown to be located in MAM and overexpression of APP has been shown to promote MAM formation both in cellular and animal models of AD (33, 44, 60). In MAMs, APP and in particular its C99 fragment is then processed by presenilin 1 and 2 into Aß proteins (45), therefore our results explain, at least in part, the increase in Aß expression in the colon and faeces of SAMP8 mice found by Pellegrini and colleagues (24). Taken as a whole, these results show that ER-mitochondria associations occur in the ENS, and damage made to MAM signalling is consistent between the neurons of the CNS and the ENS.

Despite the apparent damage made to ER-mitochondria associations and MAM signalling found in AD, data on patients are still scarce and conflicting and the pathological mechanisms are still poorly understood. Up to now only two studies, including one of ours, have attempted to study MAM from AD post-mortem tissues (61, 62). Using electronic microscopy Leal et al, showed that ER-mitochondria contacts were increased in brain biopsies from cases with idiopathic normal pressure hydrocephalus patients (62). This work had two main limitations however: first, of the 14 patients analysed in this study, only two of them had AD co-morbidities (62); second, ER-mitochondria contacts were evaluated in all cell types including both neurons or glial cells (62). Using PLAs, we recently showed that ER-mitochondria contacts were significantly reduced in cortical neurons from 14 patients with moderate AD (Braak III-IV) but not in 14 cases with a more severe disorder (Braak V-VI) (61). Interestingly no change in ER-mitochondria associations were found in Purkinje neurons from the cerebellum, a spared organ in AD (63). Although these

autopsic cases showed conflicting results, they strongly suggest that ER-mitochondria associations are altered in AD (either an increase or a decrease). The reasons for these differing results are not clear and may be due to the different experimental factors, such as post-mortem delay, sample preparation, methods to quantify ER-mitochondria contacts and signalling, however, they point out the need for quantifying ER-mitochondria and MAM signalling in fresh tissue.

Conclusion

This seminal work has shown for the first time that the ER and mitochondria interact in the enteric neurons to form MAMs. We have shown that these associations share many similarities with neurons of the CNS. Thus, ER-mitochondria associations and MAM signalling in the ENS seem to be affected in a similar fashion to that observed in the CNS by age-related neurodegenerative disorders. Although more work is needed, studying the biology of the MAM in enteric neurons is not only a promising route to understand the pathological pathways involved in GI dysfunctions associated with neurodegenerative disorders but also could be predictive of alterations made to MAMs in the neurons of the CNS in patients, given the early onset of GI disorders in age-related neurodegeneration.

List of abbreviations

AD: Alzheimer's disease

AraC: cytosine ß-D-arabinofuranoside hydrochloride

α-SMA: alpha smooth actin

CNS: central nervous system

DMEM: Dulbecco's modified Eagle Medium

EM: electron microscopy

ENS: enteric nervous system

ER: endoplasmic reticulum

FBS: fetal bovine serum

GDNF: glial derived neurotrophic factor

GFAP: glial fibrillary acidic protein

GI: gastrointestinal

HBSS: Hanks balanced salt solution

IF: immunofluorescence

IHC: immunohistochemistry

IP3R: inositol 1,4,5-trisphosphate receptor

MAM: mitochondria associated ER-membrane

MFN2: mitofusin 2

Oxphos: oxidative phosphorylation

PBS: phosphate buffer saline

PD: Parkinson’s disease

PGP 9.5: Protein Gene product 9.5

PLA: Proximity Ligation Assay

PTPIP51: Protein Tyrosine Phosphatase Interacting Protein 51

RT: room temperature

Rhod2: rhodamine 2

SAMP8: Senescence Accelerated Mouse-Prone 8

SAMR: Senescence Accelerated Mouse-Resistant 1

SEM: standard error of the mean

Sig1R: Sigma-1 receptor

VAPB: Vesicle-Associated Membrane Protein-Associated Protein B

VDAC: Voltage Dependent Anion Channel

WB: Western Blot

WT: wild type

Declarations

- *Ethics approval:* This animal study was reviewed and approved by the French Standard Ethical Guidelines for Laboratory Animals (Approval number #31937-2021070815158062).
- *Consent for publication:* not applicable
- *Availability of data and materials:* all data generated or analysed during the current study are available from the corresponding authors on reasonable request.
- *Competing interests:* authors declare they have no competing interests.
- Funding: This work was supported by grants to SP from Agence Nationale de la Recherche (ANR-16-IDEX-0007) and Conseil Régional des Pays de la Loire (PO CCI 2014 FR16M20P008) and grant to PD from the « Fédération pour la Recherche sur le Cerveau (FRC) » and by the « Association AMADYS »
- *Author's contribution:* GD, MN, PD and SP designed the study. GD, JG, PD and SP wrote first drafts of the manuscript. GD, JBB, LN, TO and SP performed most experiments. JV assisted with EM experiments and analyses. All authors edited and approved the submitted manuscript.
- *Acknowledgements:* We acknowledge the IBISA MicroPICell facility (Biogenouest), a member of the National Infrastructure France-Bioimaging,

supported by the French National Research Agency (ANR-10-INBS-04). The graphical abstract was partly generated using Servier Medical Art, provided by Servier, licensed under a Creative Commons Attribution 3.0 unported license.

Supplemental material

Supplemental Figs. S1-S3: DOI.10.6084/m9.figshare.24759651

Figure Legends

Figure1 ER-mitochondria interactions occur in enteric neurons (A) Representative electron micrograph of a 3-month-old C57BL/6J mouse, showing enteric neurons (n.) of the myenteric plexus (mp.) embedded between the longitudinal smooth muscles (lm.) and the circular smooth muscles (cm.), scale bar is 2 µm. (B) is the zoomed area marked by a black box from (A) showing an isolated enteric neuron, scale bar is 1 µm. (C) is the zoomed area marked by a black box from (B) showing close associations (≤30 nm) between the ER membrane and the outer membrane of mitochondria (highlighted in red), scale bar is 500 nm. (D) Representative high resolution electron micrograph of a 3-month-old C57BL/6J mouse, showing ER-mitochondria contacts in an enteric neuron, scale bar is 200 nm. (E) is the high magnification (high mag) marked by a black box in (D) showing a MAM compartment, scale bar is 75 nm. (F) is the same image as (E) but with dotted lines indicating putative bridges between ER and mitochondria scale bar is 75 nm. (G) bar graph showing the distribution of the proportion of ER closely apposed to mitochondria (≤30 nm) in 3-month-old C57BL/6J mice (data are from 3 animals, n=137 contacts analysed from 12 enteric neurons, and analysed by a two-way ANOVA). (H) bar graph showing the distribution of the length in nm of ER apposed to mitochondria

(≤30 nm) in enteric neurons from 3-month-old C57BL/6J mice (data are from 3 animals, n=137 contacts analysed from 12 enteric neurons, and analysed by a two-way ANOVA). (I) bar graph showing the distance between ER and mitochondria in MAMs in 3-month-old male C57BL/6J mice data are from 3 animals, n=137 contacts analysed from 12 enteric neurons, and analysed by a two-way ANOVA). (J) Expression of VAPB, PTPIP51 mitofusin-2 (MFN2) or the Sigma-1 receptor (Sig1R) in the distal colon. Immunoblots are from 3-month-old C57BL/6J. Beta actin is shown as a loading control. Molecular masses in kDa are shown on the right. (K-N) Representative images demonstrating the interaction of VAPB-PTPIP51 PLAs in the distal colon from C57BL/6J mouse. Controls involved no primary antibody (K), omission of PTPIP51 (L) or VAPB (M) antibody produced no signals whereas incubation with both primary antibodies produced strong punctiform signal (N). Enteric neurons were counterstained with the neuronal marker HuD and visualized with a VIP HRP substrate. Black arrows are depicting PLA signals, images are representative from data obtained in 3 animals, scale bar is 10 μm.

Figure 2 SAMP8 mice display a loss in hippocampal neurons associated with behavioural changes (A) Representative brain sagittal sections from SAMR1 (upper panel) or SAMP8 (lower panel), the black rectangle shows a zoom of neurons in the CA3 region (right panel). Scale bar is 300 μm. (B) Representative Western blots of the expression of PGP9.5 in the hippocampus of 8-month-old mice. Beta actin is shown as a loading control. (C) Bar chart shows relative levels PGP9.5 in the SAMR1 and SAMP8 mice following quantification of immunoreactivity from Western blots. Data are from 10 animals per condition ($p<0.0001$). (D) Open-field test in 8-month-old mice. SAMR1 and SAMP8 mice locomotor activity was tested for 10 min.

Representative traces obtained from the video analysis are shown for each phenotype. The total distance travelled (left bar graph) and the time spent in the centre (right bar graph) were calculated from these traces. Data were analysed by t-test. Error bars are SEM; SAMR1= 28 animals and SAMP8= 26 animals (*p<0.05) (E) Elevated plus maze in 8-month-old mice. SAMR1 and SAMP8 mice locomotor activity was tested for 5 min. Representative traces obtained from the video analysis are shown for each phenotype. The total distance travelled (left bar graph) and the time spent in the opened arms (right bar graph) were calculated from these traces. Data were analysed by t-test. Error bars are SEM; SAMR1= 28 animals, SAMP8= 26 animals (****p= <0.0001).

Figure 3 SAMP8 mice display a loss in enteric neurons associated with gastrointestinal disorders

(A) PGP9.5 immunostaining of SAMR1 and SAMP8 myenteric plexuses. Scale bar is 50 µm. (B) Bar graph shows PGP9.5 positive cells per mm^2 for each genotype. Data were analysed by a Mann-Whitney test. Error bars are SEM; SAMR1= 6 animals (3 males and 3 females), SAMP8= 6 animals (3 males and 3 females) **p= <0.01). (C) Bar graph shows the HuD positive cells count in the myenteric plexus for each genotype. Data were analysed by a Mann-Whitney test. Error bars are SEM; SAMR1= 6 animals (3 males and 3 females), SAMP8= 6 animals (3 males and 3 females) *p= <0.05). (D) GI transit time evaluation in 8-month-old mice. SAMR1 and SAMP8 were fed with a carmine red dye and the time for the first red stool (upper cartoon) was recorded. After the test, the total gut length was measured (left bar graph). Then the total transit time was assessed and compensated by the total gut length (right bar graph). Gut length: data were analysed by t-test. Error bars are

SEM; SAMR1= 27 animals, SAMP8= 25 animals (*p<0.05). (E) Fecal pellet output evaluation in 8-month-old mice. SAMR1 and SAMP8 were put individually in a cage and stools were collected over a 2 h period (left bar graph) and the fresh stool weight was measured (right bar graph). Data were analysed by t-test. Error bars are SEM; SAMR1= 27 animals, SAMP8= 26 animals (*p< 0.05 for fecal pellet output; **p< 0.01 for fresh stool weight). Animals which did not produce stools were removed from the statistical analysis.

Figure 4 ER-mitochondria associations are increased in the distal colon of SAMP8 mice at 8 months (A) Representative electron micrographs showing ER-mitochondria contacts (red lines indicate distance of interaction ≤30 nm) in the enteric neurons of an 8-month-old SAMR1 distal colon (left panel) and 8-month-old SAMP8 distal colon (right panel) (scale bar is 100 nm). (B) Bar graph representing the percentage of the mitochondrial membrane in contact with ER in the enteric neurons of SAMR1 and SAMP8 mice at the age of 8 months. Data were analysed by t-test. Error bars are SEM; SAMR1 n=189 contacts, SAMP8 n=192 contacts from 6 animals per condition with 4 to 6 cells analysed per animal. (****p<0.0001). (C) Bar graph representing the average ER-mitochondria contact length in the enteric neurons of SAMR1 and SAMP8 mice at the age of 8 months. Data were analysed by t-test. SAMR1 n=189 contacts, SAMP8 n=192 contacts from 6 animals per condition. ***p=0.001). (D) Bar graph representing the space in nm separating ER and mitochondria within the MAMs in the enteric neurons of SAMR1 and SAMP8 mice at the age of 8 months. Data were analysed by t-test. SAMR1 n=189 contacts, SAMP8 n=192 contacts from 6 animals per condition. (NS p=0.0567). (E) bar graph representing the mitochondria surface area in nm^2 in 8-month-old SAMR1 and SAMP8 mice. Data are from 6

animals per condition SAMR1 n=189 contacts, SAMP8 n=192 contacts and were analysed by t-test. (F) bar graph representing the distribution of the proportion of ER closely apposed to mitochondria in 8-month-old SAMR1 and SAMP8 mice. Data are from 6 animals per condition SAMR1 n=189 contacts, SAMP8 n=192 contacts and were analysed by a two-way ANOVA. (G) Bar graph representing the distribution of the length in nm of ER apposed to mitochondria (≤30 nm) in enteric neurons from 8-month-old SAMR1 and SAMP8. Data are from 6 animals per condition SAMR1 n=189 contacts, SAMP8 n=192 contacts and were analysed by a two-way ANOVA. (H) bar graph representing the distance between ER and mitochondria in MAMs in 8-month-old SAMR1 and SAMP8 mice. Data are from 6 animals per condition SAMR1 n=189 contacts, SAMP8 n=192 contacts were analysed by a two-way ANOVA.

Figure 5 MAM signalling is altered in the enteric neurons in age-related neurodegeneration (A) Representative immunoblots of VAPB, PTPIP51 and MF2 from enteric neuron enriched primary cultures after 15 days of culture. (n=10 for SAMR1 and 8 for SAMP8 culture wells from 8 to 10 independent mouse embryos). Beta actin is shown as a loading control. Molecular masses in kDa are shown on the right. Bar graphs show the relative levels of VAPB (B), PTPIP51, (C) and MFN2 (D) (data are from 3 different cultures, $p>0.05$). (E) ER–mitochondria Ca^{2+} exchange is increased in SAMP8 neurons. ER–mitochondrial Ca^{2+} exchange following IP3 receptor-mediated release from ER-stores in SAMR1 and SAMP8 primary enteric neurons. IP3 receptor mediated Ca^{2+} release was triggered with 100 µM of OxoM and mitochondrial Ca^{2+} levels detected by Rhod2 fluorescence. Representative Rhod2 fluorescence traces are shown (E) with maximum peak values (Fmax/F0) in the bar chart (F). Data were analysed by unpaired t-test. SAMR1 n=79 neurons,

SAMP8 n=43 neurons from 3 different experiments; error bars are SEM (*** $p < 0.0001$).

References

1. **Markovinovic A**, **Greig J**, **Martín-Guerrero SM**, **Salam S**, **Paillusson S**. Endoplasmic reticulum-mitochondria signaling in neurons and neurodegenerative diseases. *J Cell Sci* 135: jcs248534, 2022. doi: 10.1242/jcs.248534.

2. **Csordás G**, **Renken C**, **Várnai P**, **Walter L**, **Weaver D**, **Buttle KF**, **Balla T**, **Mannella CA**, **Hajnóczky G**. Structural and functional features and significance of the physical linkage between ER and mitochondria. *J Cell Biol* 174: 915–921, 2006. doi: 10.1083/jcb.200604016.

3. **Kornmann B**, **Currie E**, **Collins SR**, **Schuldiner M**, **Nunnari J**, **Weissman JS**, **Walter P**. An ER-mitochondria tethering complex revealed by a synthetic biology screen. *Science* 325: 477–481, 2009. doi: 10.1126/science.1175088.

4. **Csordás G**, **Weaver D**, **Hajnóczky G**. Endoplasmic Reticulum-Mitochondrial Contactology: Structure and Signaling Functions. *Trends Cell Biol* 28: 523–540, 2018. doi: 10.1016/j.tcb.2018.02.009.

5. **Chapelet G**, **Leclair-Visonneau L**, **Clairembault T**, **Neunlist M**, **Derkinderen P**. Can the gut be the missing piece in uncovering PD pathogenesis? *Parkinsonism Relat Disord* 59: 26–31, 2019. doi: 10.1016/j.parkreldis.2018.11.014.

6. **Boehme M**, **Guzzetta KE**, **Wasén C**, **Cox LM**. The gut microbiota is an emerging target for improving brain health during ageing. *Gut Microbiome (Camb)* 4: E2, 2023. doi: 10.1017/gmb.2022.11.

7. **Rao M**, **Gershon MD**. The bowel and beyond: the enteric nervous system in neurological disorders. *Nat Rev Gastroenterol Hepatol* 13: 517–528, 2016. doi: 10.1038/nrgastro.2016.107.

8. **Sharkey KA**, **Mawe GM**. The enteric nervous system. *Physiol Rev* 103: 1487–1564, 2023. doi: 10.1152/physrev.00018.2022.

9. **Caillaud M**, **Le Dréan ME**, **De-Guilhem-de-Lataillade A**, **Le Berre-Scoul C**, **Montnach J**, **Nedellec S**, **Loussouarn G**, **Paillé V**, **Neunlist M**, **Boudin H**. A functional network of highly pure enteric neurons in a dish. *Front Neurosci* 16: 1062253, 2023. doi: 10.3389/fnins.2022.1062253.

10. **Tasselli M**, **Chaumette T**, **Paillusson S**, **Monnet Y**, **Lafoux A**, **Huchet-Cadiou C**, **Aubert P**, **Hunot S**, **Derkinderen P**, **Neunlist M**. Effects of oral administration of rotenone on gastrointestinal functions in mice. *Neurogastroenterology & Motility* 25: e183–e193, 2013. doi: 10.1111/nmo.12070.

11. **Paillusson S**, **Gomez-Suaga P**, **Stoica R**, **Little D**, **Gissen P**, **Devine MJ**, **Noble W**, **Hanger DP**, **Miller CCJ**. α-Synuclein binds to the ER-mitochondria tethering protein VAPB to disrupt Ca2+ homeostasis and mitochondrial ATP production. *Acta Neuropathol* 134: 129–149, 2017. doi: 10.1007/s00401-017-1704-z.

12. **Klüver H**, **Barrera E**. A Method for the Combined Staining of Cells and Fibers in the Nervous System*. *Journal of Neuropathology & Experimental Neurology* 12: 400–403, 1953. doi: 10.1097/00005072-195312040-00008.

13. **Stoica R**, **De Vos KJ**, **Paillusson S**, **Mueller S**, **Sancho RM**, **Lau K-F**, **Vizcay-Barrena G**, **Lin W-L**, **Xu Y-F**, **Lewis J**, **Dickson DW**, **Petrucelli L**, **Mitchell JC**, **Shaw CE**, **Miller CCJ**. ER–mitochondria associations are regulated by the VAPB–PTPIP51 interaction and are disrupted by ALS/FTD-associated TDP-43. *Nat Commun* 5, 2014. doi: 10.1038/ncomms4996.

14. **Gómez-Suaga P**, **Pérez-Nievas BG**, **Glennon EB**, **Lau DHW**, **Paillusson S**, **Mórotz GM**, **Calì T**, **Pizzo P**, **Noble W**, **Miller CCJ**. The VAPB-PTPIP51 endoplasmic reticulum-mitochondria tethering proteins are present in neuronal synapses and regulate synaptic activity. *Acta Neuropathol Commun* 7, 2019. doi: 10.1186/s40478-019-0688-4.

15. **De Vos KJ**, **Mórotz GM**, **Stoica R**, **Tudor EL**, **Lau K-F**, **Ackerley S**, **Warley A**, **Shaw CE**, **Miller CCJ**. VAPB interacts with the mitochondrial protein PTPIP51 to regulate calcium homeostasis. *Hum Mol Genet* 21: 1299–1311, 2012. doi: 10.1093/hmg/ddr559.

16. **Gomez-Suaga P**, **Paillusson S**, **Stoica R**, **Noble W**, **Hanger DP**, **Miller CCJ**. The ER-Mitochondria Tethering Complex VAPB-PTPIP51 Regulates Autophagy. *Curr Biol* 27: 371–385, 2017. doi: 10.1016/j.cub.2016.12.038.

17. **Hamasaki M**, **Furuta N**, **Matsuda A**, **Nezu A**, **Yamamoto A**, **Fujita N**, **Oomori H**, **Noda T**, **Haraguchi T**, **Hiraoka Y**, **Amano A**, **Yoshimori T**. Autophagosomes form at ER-mitochondria contact sites. *Nature* 495: 389–393, 2013. doi: 10.1038/nature11910.

18. **de Brito OM**, **Scorrano L**. Mitofusin 2 tethers endoplasmic reticulum to mitochondria. *Nature* 456: 605–610, 2008. doi: 10.1038/nature07534.

19. **Hayashi T**, **Su T-P**. Sigma-1 receptor chaperones at the ER-mitochondrion interface regulate Ca(2+) signaling and cell survival. *Cell* 131: 596–610, 2007. doi: 10.1016/j.cell.2007.08.036.

20. **Stoica R**, **Paillusson S**, **Gomez-Suaga P**, **Mitchell JC**, **Lau DH**, **Gray EH**, **Sancho RM**, **Vizcay-Barrena G**, **De Vos KJ**, **Shaw CE**, **Hanger DP**, **Noble W**, **Miller CC**. ALS/FTD-associated FUS activates GSK-3β to disrupt the VAPB-PTPIP51 interaction and ER-mitochondria associations. *EMBO Rep* 17: 1326–1342, 2016. doi: 10.15252/embr.201541726.

21. **Cieri D**, **Vicario M**, **Giacomello M**, **Vallese F**, **Filadi R**, **Wagner T**, **Pozzan T**, **Pizzo P**, **Scorrano L**, **Brini M**, **Calì T**. SPLICS: a split green fluorescent protein-based contact site sensor for narrow and wide heterotypic organelle juxtaposition. *Cell Death Differ* 25: 1131–1145, 2018. doi: 10.1038/s41418-017-0033-z.

22. **Takeda T**, **Hosokawa M**, **Higuchi K**. Senescence-accelerated mouse (SAM): a novel murine model of accelerated senescence. *J Am Geriatr Soc* 39: 911–919, 1991. doi: 10.1111/j.1532-5415.1991.tb04460.x.

23. **Akiguchi I**, **Pallàs M**, **Budka H**, **Akiyama H**, **Ueno M**, **Han J**, **Yagi H**, **Nishikawa T**, **Chiba Y**, **Sugiyama H**, **Takahashi R**, **Unno K**, **Higuchi K**, **Hosokawa M**. SAMP8 mice as a neuropathological model of accelerated brain aging and dementia: Toshio Takeda's legacy and future directions. *Neuropathology* 37: 293–305, 2017. doi: 10.1111/neup.12373.

24. **Pellegrini C**, **Daniele S**, **Antonioli L**, **Benvenuti L**, **D'Antongiovanni V**, **Piccarducci R**, **Pietrobono D**, **Citi V**, **Piragine E**, **Flori L**, **Ippolito C**, **Segnani C**, **Palazon-Riquelme P**, **Lopez-Castejon G**, **Martelli A**, **Colucci R**, **Bernardini N**, **Trincavelli ML**, **Calderone V**, **Martini C**, **Blandizzi C**, **Fornai M**. Prodromal Intestinal Events in Alzheimer's Disease (AD): Colonic Dysmotility and Inflammation Are Associated with Enteric AD-Related Protein Deposition. *Int J Mol Sci* 21: E3523, 2020. doi: 10.3390/ijms21103523.

25. **Li G**, **Cheng H**, **Zhang X**, **Shang X**, **Xie H**, **Zhang X**, **Yu J**, **Han J**. Hippocampal neuron loss is correlated with cognitive deficits in SAMP8 mice. *Neurol Sci* 34: 963–969, 2013. doi: 10.1007/s10072-012-1173-z.

26. **Morley JE**, **Kumar VB**, **Bernardo AE**, **Farr SA**, **Uezu K**, **Tumosa N**, **Flood JF**. Beta-amyloid precursor polypeptide in SAMP8 mice affects learning and memory. *Peptides* 21: 1761–1767, 2000. doi: 10.1016/s0196-9781(00)00342-9.

27. **Bartolome F**, **Wu H-C**, **Burchell VS**, **Preza E**, **Wray S**, **Mahoney CJ**, **Fox NC**, **Calvo A**, **Canosa A**, **Moglia C**, **Mandrioli J**, **Chiò A**, **Orrell RW**, **Houlden H**, **Hardy J**, **Abramov AY**, **Plun-Favreau H**. Pathogenic VCP Mutations Induce Mitochondrial Uncoupling and Reduced ATP Levels. *Neuron* 78: 57–64, 2013. doi: 10.1016/j.neuron.2013.02.028.

28. **Kruman II**, **Mattson MP**. Pivotal Role of Mitochondrial Calcium Uptake in Neural Cell Apoptosis and Necrosis. *Journal of Neurochemistry* 72: 529–540, 1999. doi: 10.1046/j.1471-4159.1999.0720529.x.

29. **Lim D**, **Dematteis G**, **Tapella L**, **Genazzani AA**, **Calì T**, **Brini M**, **Verkhratsky A**. Ca2+ handling at the mitochondria-ER contact sites in neurodegeneration. *Cell Calcium* 98: 102453, 2021. doi: 10.1016/j.ceca.2021.102453.

30. **Lee K-S**, **Huh S**, **Lee S**, **Wu Z**, **Kim A-K**, **Kang H-Y**, **Lu B**. Altered ER–mitochondria contact impacts mitochondria calcium homeostasis and contributes to neurodegeneration in vivo in disease models. *Proceedings of the National Academy of Sciences* 115: E8844–E8853, 2018. doi: 10.1073/pnas.1721136115.

31. **Gomez-Suaga P**, **Mórotz GM**, **Markovinovic A**, **Martín-Guerrero SM**, **Preza E**, **Arias N**, **Mayl K**, **Aabdien A**, **Gesheva V**, **Nishimura A**, **Annibali A**, **Lee Y**, **Mitchell JC**, **Wray S**, **Shaw C**, **Noble W**, **Miller CCJ**. Disruption of ER-mitochondria tethering and signalling in C9orf72-associated amyotrophic lateral sclerosis and frontotemporal dementia. .

32. **Schemann M**, **Neunlist M**. The human enteric nervous system. *Neurogastroenterol Motil* 16 Suppl 1: 55–59, 2004. doi: 10.1111/j.1743-3150.2004.00476.x.

33. **Leal NS**, **Dentoni G**, **Schreiner B**, **Naia L**, **Piras A**, **Graff C**, **Cattaneo A**, **Meli G**, **Hamasaki M**, **Nilsson P**, **Ankarcrona M**. Amyloid β-Peptide Increases Mitochondria-Endoplasmic Reticulum Contact Altering Mitochondrial Function and Autophagosome Formation in Alzheimer's Disease-Related Models. *Cells* 9: 2552, 2020. doi: 10.3390/cells9122552.

34. **Del Valle J**, **Duran-Vilaregut J**, **Manich G**, **Casadesús G**, **Smith MA**, **Camins A**, **Pallàs M**, **Pelegrí C**, **Vilaplana J**. Early amyloid accumulation in the hippocampus of SAMP8 mice. *J Alzheimers Dis* 19: 1303–1315, 2010. doi: 10.3233/JAD-2010-1321.

35. **Manich G**, **Mercader C**, **del Valle J**, **Duran-Vilaregut J**, **Camins A**, **Pallàs M**, **Vilaplana J**, **Pelegrí C**. Characterization of amyloid-β granules in the hippocampus of SAMP8 mice. *J Alzheimers Dis* 25: 535–546, 2011. doi: 10.3233/JAD-2011-101713.

36. **Joachim CL**, **Mori H**, **Selkoe DJ**. Amyloid beta-protein deposition in tissues other than brain in Alzheimer's disease. *Nature* 341: 226–230, 1989. doi: 10.1038/341226a0.

37. **Puig KL**, **Lutz BM**, **Urquhart SA**, **Rebel AA**, **Zhou X**, **Manocha GD**, **Sens M**, **Tuteja AK**, **Foster NL**, **Combs CK**. Overexpression of Mutant Amyloid-β Protein Precursor and Presenilin 1 Modulates Enteric Nervous System. *J Alzheimers Dis* 44: 1263–1278, 2015. doi: 10.3233/JAD-142259.

38. **Kakuda N**, **Miyasaka T**, **Iwasaki N**, **Nirasawa T**, **Wada-Kakuda S**, **Takahashi-Fujigasaki J**, **Murayama S**, **Ihara Y**, **Ikegawa M**. Distinct deposition of amyloid-β species in brains with Alzheimer's disease pathology visualized with MALDI imaging mass spectrometry. *Acta Neuropathologica Communications* 5: 73, 2017. doi: 10.1186/s40478-017-0477-x.

39. **Nakase T**, **Tatewaki Y**, **Thyreau B**, **Mutoh T**, **Tomita N**, **Yamamoto S**, **Takano Y**, **Muranaka M**, **Taki Y**. Impact of constipation on progression of Alzheimer's disease: A retrospective study. *CNS Neuroscience & Therapeutics* 28: 1964–1973, 2022. doi: 10.1111/cns.13940.

40. **Fasano A**, **Visanji NP**, **Liu LWC**, **Lang AE**, **Pfeiffer RF**. Gastrointestinal dysfunction in Parkinson's disease. *Lancet Neurol* 14: 625–639, 2015. doi: 10.1016/S1474-4422(15)00007-1.

41. **Kumar VB**, **Vyas K**, **Franko M**, **Choudhary V**, **Buddhiraju C**, **Alvarez J**, **Morley JE**. Molecular cloning, expression, and regulation of hippocampal amyloid precursor protein of senescence accelerated mouse (SAMP8). *Biochem Cell Biol* 79: 57–67, 2001. doi: 10.1139/o00-094.

42. **Delay C**, **Calon F**, **Mathews P**, **Hébert SS**. Alzheimer-specific variants in the 3'UTR of Amyloid precursor protein affect microRNA function. *Molecular Neurodegeneration* 6: 70, 2011. doi: 10.1186/1750-1326-6-70.

43. **Area-Gomez E**, **Castillo M del CL**, **Tambini MD**, **Guardia-Laguarta C**, **Groof AJC de**, **Madra M**, **Ikenouchi J**, **Umeda M**, **Bird TD**, **Sturley SL**, **Schon EA**. Upregulated function of mitochondria-associated ER membranes in Alzheimer

disease. *The EMBO Journal* 31: 4106, 2012. doi: 10.1038/emboj.2012.202.

44. **Hedskog L**, **Pinho CM**, **Filadi R**, **Rönnbäck A**, **Hertwig L**, **Wiehager B**, **Larssen P**, **Gellhaar S**, **Sandebring A**, **Westerlund M**, **Graff C**, **Winblad B**, **Galter D**, **Behbahani H**, **Pizzo P**, **Glaser E**, **Ankarcrona M**. Modulation of the endoplasmic reticulum–mitochondria interface in Alzheimer's disease and related models. *Proceedings of the National Academy of Sciences* 110: 7916–7921, 2013. doi: 10.1073/pnas.1300677110.

45. **Pera M**, **Larrea D**, **Guardia-Laguarta C**, **Montesinos J**, **Velasco KR**, **Agrawal RR**, **Xu Y**, **Chan RB**, **Di Paolo G**, **Mehler MF**, **Perumal GS**, **Macaluso FP**, **Freyberg ZZ**, **Acin-Perez R**, **Enriquez JA**, **Schon EA**, **Area-Gomez E**. Increased localization of APP-C99 in mitochondria-associated ER membranes causes mitochondrial dysfunction in Alzheimer disease. *The EMBO Journal* 36: 3356–3371, 2017. doi: 10.15252/embj.201796797.

46. **Mizutani J**, **Chiba T**, **Tanaka M**, **Higuchi K**, **Mori M**. Unique Mutations in Mitochondrial DNA of Senescence-Accelerated Mouse (SAM) Strains. *Journal of Heredity* 92: 352–355, 2001. doi: 10.1093/jhered/92.4.352.

47. **Bharucha AE**, **Lacy BE**. Mechanisms, Evaluation, and Management of Chronic Constipation. *Gastroenterology* 158: 1232-1249.e3, 2020. doi: 10.1053/j.gastro.2019.12.034.

48. **Bassotti G**, **Villanacci V**, **Creţoiu D**, **Creţoiu SM**, **Becheanu G**. Cellular and molecular basis of chronic constipation: taking the functional/idiopathic label out. *World J Gastroenterol* 19: 4099–4105, 2013. doi: 10.3748/wjg.v19.i26.4099.

49. **Wattchow D**, **Brookes S**, **Murphy E**, **Carbone S**, **de Fontgalland D**, **Costa M**. Regional variation in the neurochemical coding of the myenteric plexus of the human colon and changes in patients with slow transit constipation. *Neurogastroenterol Motil* 20: 1298–1305, 2008. doi: 10.1111/j.1365-2982.2008.01165.x.

50. **Wedel T**, **Roblick UJ**, **Ott V**, **Eggers R**, **Schiedeck THK**, **Krammer H-J**, **Bruch H-P**. Oligoneuronal hypoganglionosis in patients with idiopathic slow-transit constipation. *Dis Colon Rectum* 45: 54–62, 2002. doi: 10.1007/s10350-004-6114-3.

51. **Fung C**, **Vanden Berghe P**. Functional circuits and signal processing in the enteric nervous system. *Cell Mol Life Sci* 77: 4505–4522, 2020. doi: 10.1007/s00018-020-03543-6.

52. **De Giorgio R**, **Bianco F**, **Latorre R**, **Caio G**, **Clavenzani P**, **Bonora E**. Enteric neuropathies: Yesterday, Today and Tomorrow. *Adv Exp Med Biol* 891: 123–133, 2016. doi: 10.1007/978-3-319-27592-5_12.

53. **de Guilhem de Lataillade A**, **Lebouvier T**, **Noble W**, **Leclair-Visonneau L**, **Derkinderen P**. Enteric synucleinopathy: from trendy concept to real entity. *Free Neuropathol* 1: 1–26, 2020. doi: 10.17879/freeneuropathology-2020-2920.

54. **Fu P**, **Gao M**, **Yung KKL**. Association of Intestinal Disorders with Parkinson's

Disease and Alzheimer's Disease: A Systematic Review and Meta-Analysis. *ACS Chem Neurosci* 11: 395–405, 2020. doi: 10.1021/acschemneuro.9b00607.

55. **Caušević M**, **Farooq U**, **Lovestone S**, **Killick R**. β-Amyloid precursor protein and tau protein levels are differently regulated in human cerebellum compared to brain regions vulnerable to Alzheimer's type neurodegeneration. *Neurosci Lett* 485: 162–166, 2010. doi: 10.1016/j.neulet.2010.08.088.

56. **Braak H**, **Alafuzoff I**, **Arzberger T**, **Kretzschmar H**, **Del Tredici K**. Staging of Alzheimer disease-associated neurofibrillary pathology using paraffin sections and immunocytochemistry. *Acta Neuropathol* 112: 389–404, 2006. doi: 10.1007/s00401-006-0127-z.

57. **Tavares IA**, **Touma D**, **Lynham S**, **Troakes C**, **Schober M**, **Causevic M**, **Garg R**, **Noble W**, **Killick R**, **Bodi I**, **Hanger DP**, **Morris JDH**. Prostate-derived sterile 20-like kinases (PSKs/TAOKs) phosphorylate tau protein and are activated in tangle-bearing neurons in Alzheimer disease. *J Biol Chem* 288: 15418–15429, 2013. doi: 10.1074/jbc.M112.448183.

58. **Mórotz GM**, **Glennon EB**, **Gomez-Suaga P**, **Lau DHW**, **Robinson ED**, **Sedlák É**, **Vagnoni A**, **Noble W**, **Miller CCJ**. LMTK2 binds to kinesin light chains to mediate anterograde axonal transport of cdk5/p35 and LMTK2 levels are reduced in Alzheimer's disease brains. *Acta Neuropathol Commun* 7: 73, 2019. doi: 10.1186/s40478-019-0715-5.

59. **Takemura M**, **Nakamura S**, **Akiguchi I**, **Ueno M**, **Oka N**, **Ishikawa S**, **Shimada A**, **Kimura J**, **Takeda T**. Beta/A4 proteinlike immunoreactive granular structures in the brain of senescence-accelerated mouse. *Am J Pathol* 142: 1887–1897, 1993.

60. **Del Prete D**, **Suski JM**, **Oulès B**, **Debayle D**, **Gay AS**, **Lacas-Gervais S**, **Bussiere R**, **Bauer C**, **Pinton P**, **Paterlini-Bréchot P**, **Wieckowski MR**, **Checler F**, **Chami M**. Localization and Processing of the Amyloid-β Protein Precursor in Mitochondria-Associated Membranes. *Journal of Alzheimer's Disease* 55: 1549–1570, 2017. doi: 10.3233/JAD-160953.

61. **Lau DHW**, **Paillusson S**, **Hartopp N**, **Rupawala H**, **Mórotz GM**, **Gomez-Suaga P**, **Greig J**, **Troakes C**, **Noble W**, **Miller CCJ**. Disruption of endoplasmic reticulum-mitochondria tethering proteins in post-mortem Alzheimer's disease brain. *Neurobiol Dis* 143: 105020, 2020. doi: 10.1016/j.nbd.2020.105020.

62. **Leal NS**, **Dentoni G**, **Schreiner B**, **Kämäräinen O-P**, **Partanen N**, **Herukka S-K**, **Koivisto AM**, **Hiltunen M**, **Rauramaa T**, **Leinonen V**, **Ankarcrona M**. Alterations in mitochondria-endoplasmic reticulum connectivity in human brain biopsies from idiopathic normal pressure hydrocephalus patients. *Acta Neuropathol Commun* 6: 102, 2018. doi: 10.1186/s40478-018-0605-2.

63. **Andersen K**, **Andersen BB**, **Pakkenberg B**. Stereological quantification of the cerebellum in patients with Alzheimer's disease. *Neurobiol Aging* 33: 197.e11–20, 2012. doi: 10.1016/j.neurobiolaging.2010.06.013.

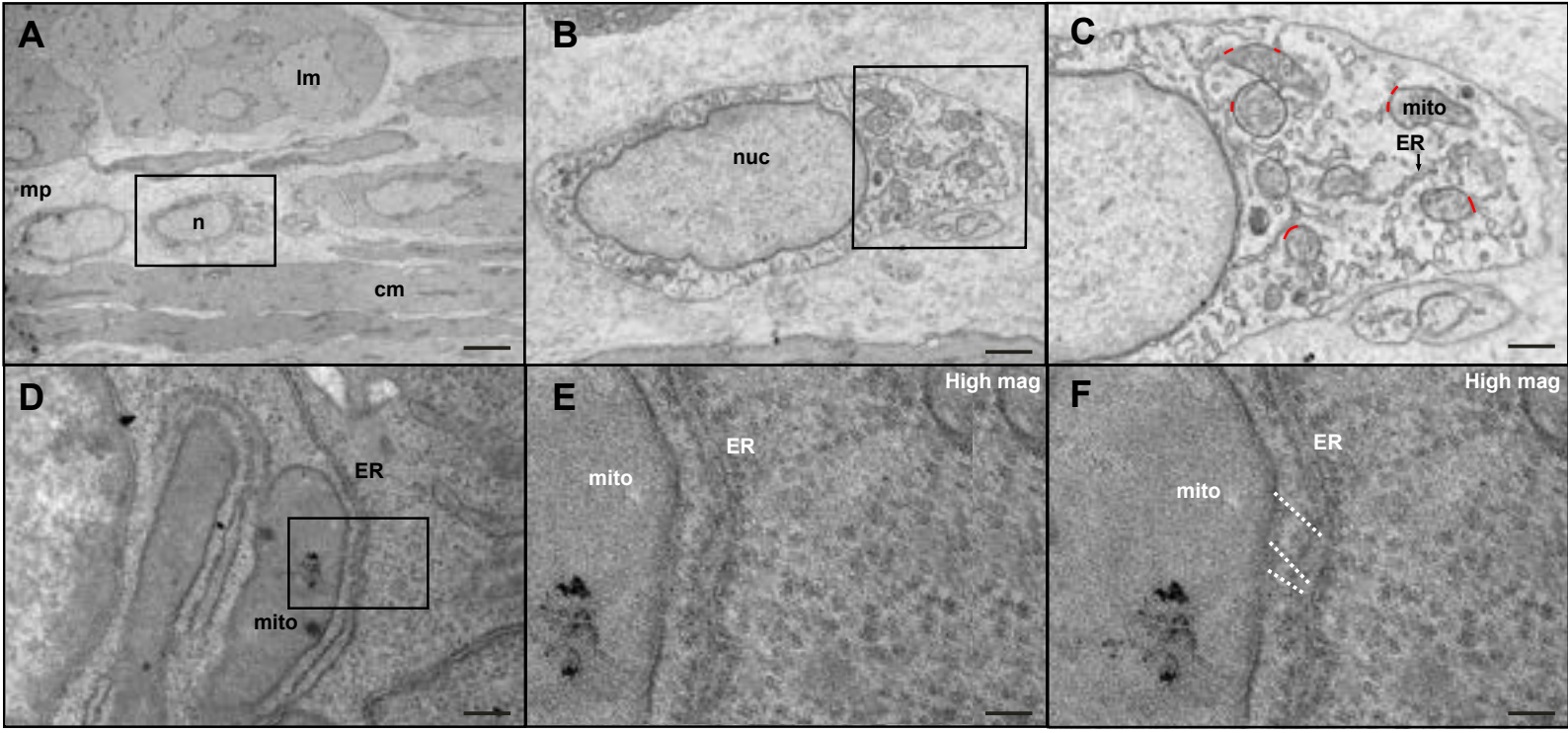
A
lm
mp
n
cm
B
nuc
C
mito
ER
D
ER
mito
E
High mag
ER
mito
F
High mag
ER
mito

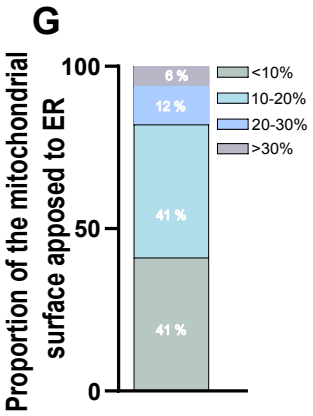
G
Proportion of the mitochondrial surface apposed to ER
100
50
0
6 %
12 %
41 %
41 %
<10%
10-20%
20-30%
>30%

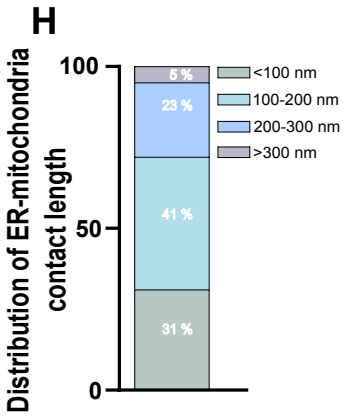
H
Distribution of ER-mitochondria contact length
100
50
0
5 %
23 %
41 %
31 %
<100 nm
100-200 nm
200-300 nm
>300 nm

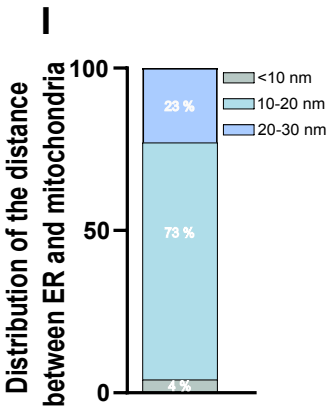
I
Distribution of the distance between ER and mitochondria
100
50
0
23 %
73 %
4 %
<10 nm
10-20 nm
20-30 nm

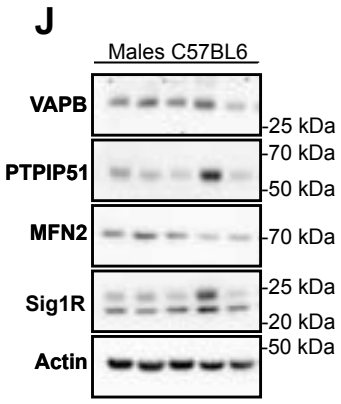
J
Males C57BL6
VAPB
PTPIP51
MFN2
Sig1R
Actin
25 kDa
70 kDa
50 kDa
70 kDa
25 kDa
20 kDa
50 kDa

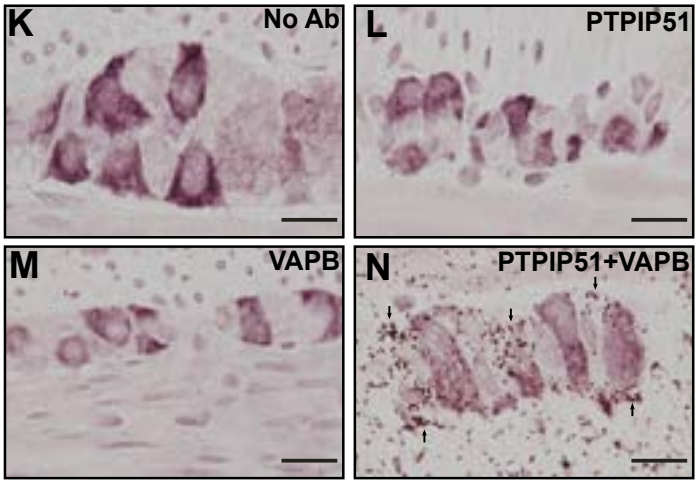
K
No Ab
L
PTPIP51
M
VAPB
N
PTPIP51+VAPB

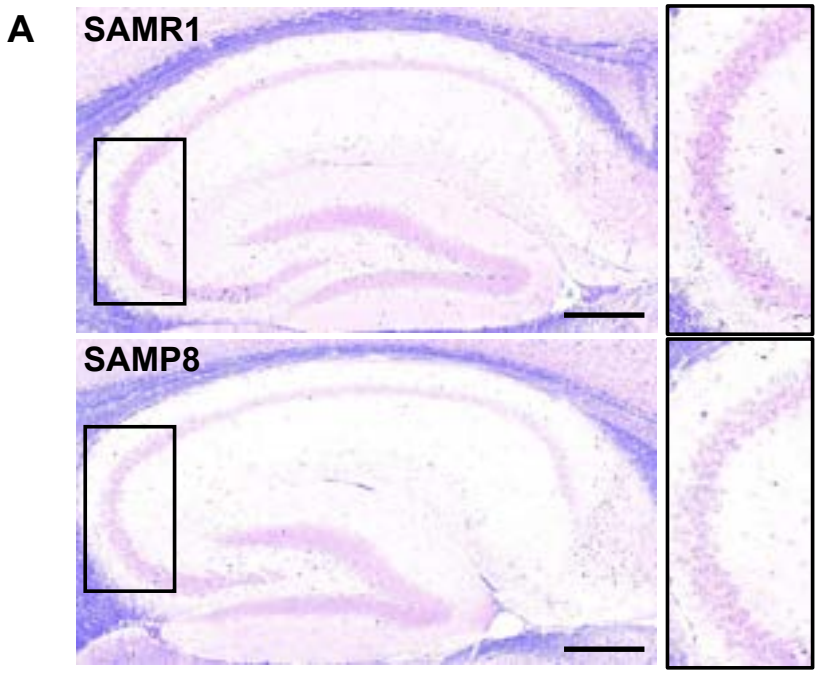
A
SAMR1
SAMP8

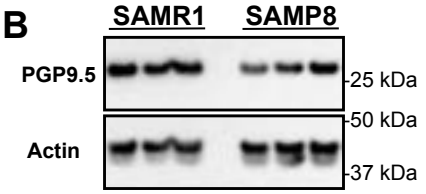
B
SAMR1
SAMP8
PGP9.5
Actin
25 kDa
50 kDa
37 kDa

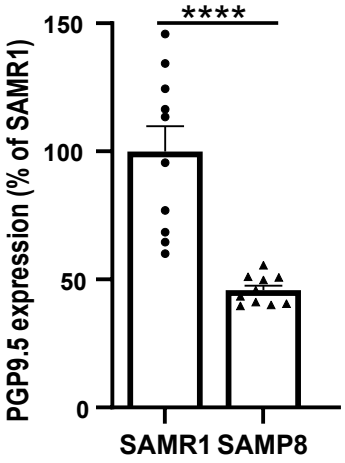
C
****
PGP9.5 expression (% of SAMR1)
150
100
50
0
SAMR1 SAMP8

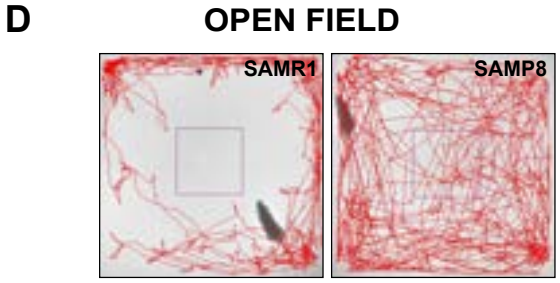
D
OPEN FIELD
SAMR1
SAMP8

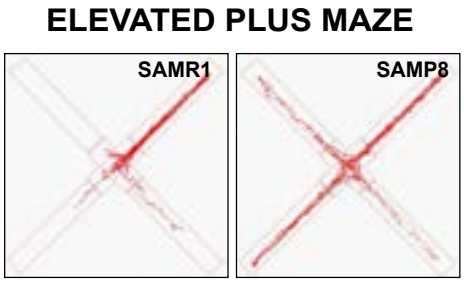
E
ELEVATED PLUS MAZE
SAMR1
SAMP8

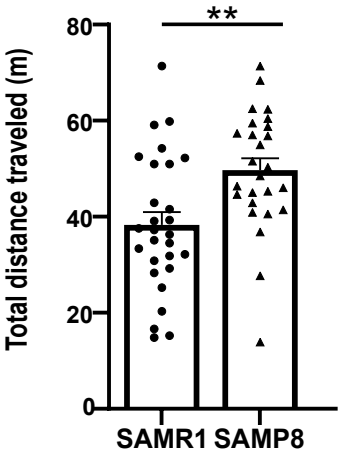
**
Total distance traveled (m)
80
60
40
20
0
SAMR1 SAMP8

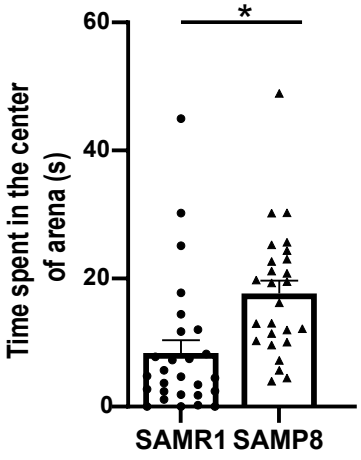
*
Time spent in the center of arena (s)
60
40
20
0
SAMR1 SAMP8

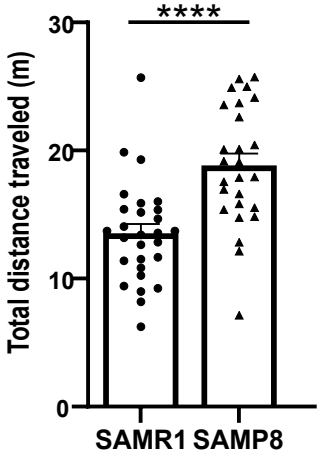
****
Total distance traveled (m)
30
20
10
0
SAMR1 SAMP8

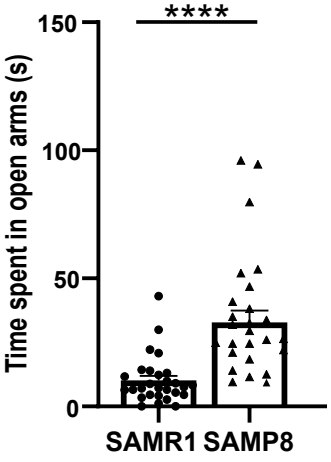
****
Time spent in open arms (s)
150
100
50
0
SAMR1 SAMP8

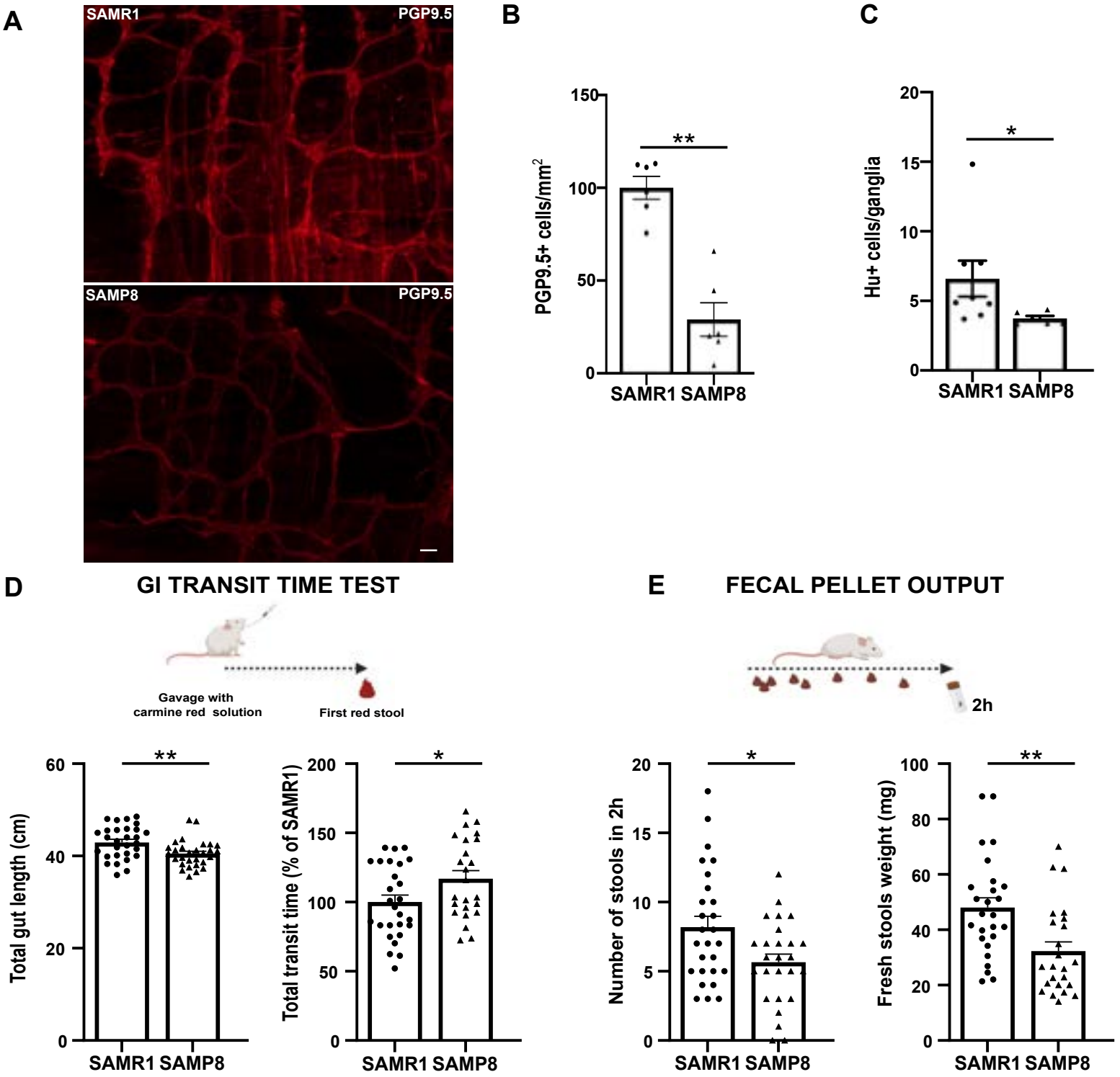
A
SAMR1
PGP9.5
SAMP8
PGP9.5
B
PGP9.5+ cells/mm2
150
100
50
0
**
SAMR1 SAMP8
C
Hu+ cells/ganglia
20
15
10
5
0
*
SAMR1 SAMP8
D
GI TRANSIT TIME TEST
Gavage with
carmine red solution
First red stool
Total gut length (cm)
60
40
20
0
**
SAMR1 SAMP8
Total transit time (% of SAMR1)
200
150
100
50
0
*
SAMR1 SAMP8
E
FECAL PELLET OUTPUT
2h
Number of stools in 2h
20
15
10
5
0
*
SAMR1 SAMP8
Fresh stools weight (mg)
100
80
60
40
20
0
**
SAMR1 SAMP8

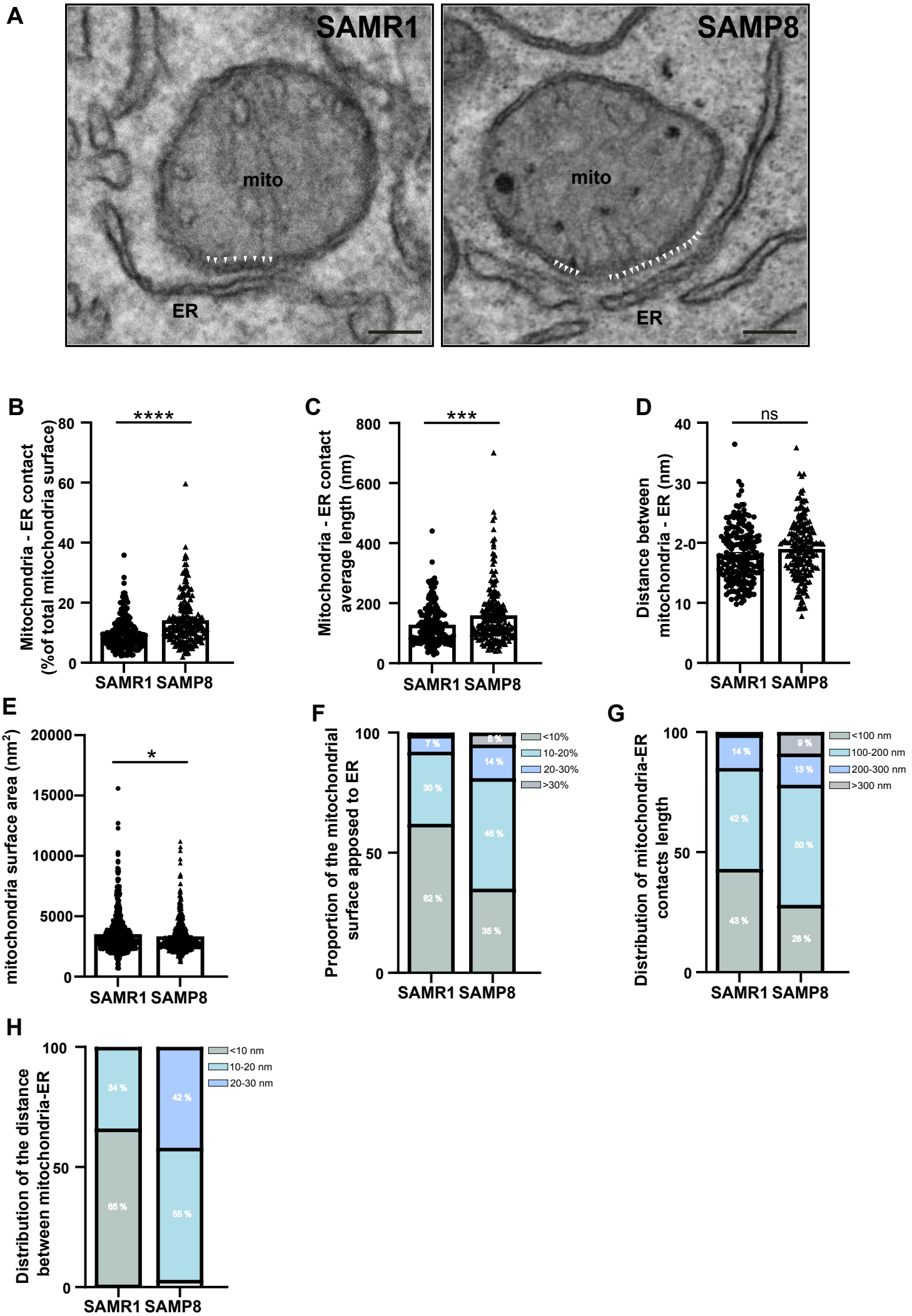
A
SAMR1
mito
ER
SAMP8
mito
ER
B
****
Mitochondria - ER contact (%of total mitochondria surface)
0
20
40
60
80
SAMR1 SAMP8
C
***
Mitochondria - ER contact average length (nm)
0
200
400
600
800
SAMR1 SAMP8
D
ns
Distance between mitochondria - ER (nm)
0
10
2-0
30
40
SAMR1 SAMP8
E
*
mitochondria surface area (nm2)
0
5000
10000
15000
20000
SAMR1 SAMP8
F
Proportion of the mitochondrial surface apposed to ER
0
50
100
7 %
30 %
62 %
5 %
14 %
46 %
35 %
<10%
10-20%
20-30%
>30%
SAMR1 SAMP8
G
Distribution of mitochondria-ER contacts length
0
50
100
14 %
42 %
43 %
9 %
13 %
50 %
28 %
<100 nm
100-200 nm
200-300 nm
>300 nm
SAMR1 SAMP8
H
Distribution of the distance between mitochondria-ER
0
50
100
34 %
65 %
42 %
55 %
<10 nm
10-20 nm
20-30 nm
SAMR1 SAMP8

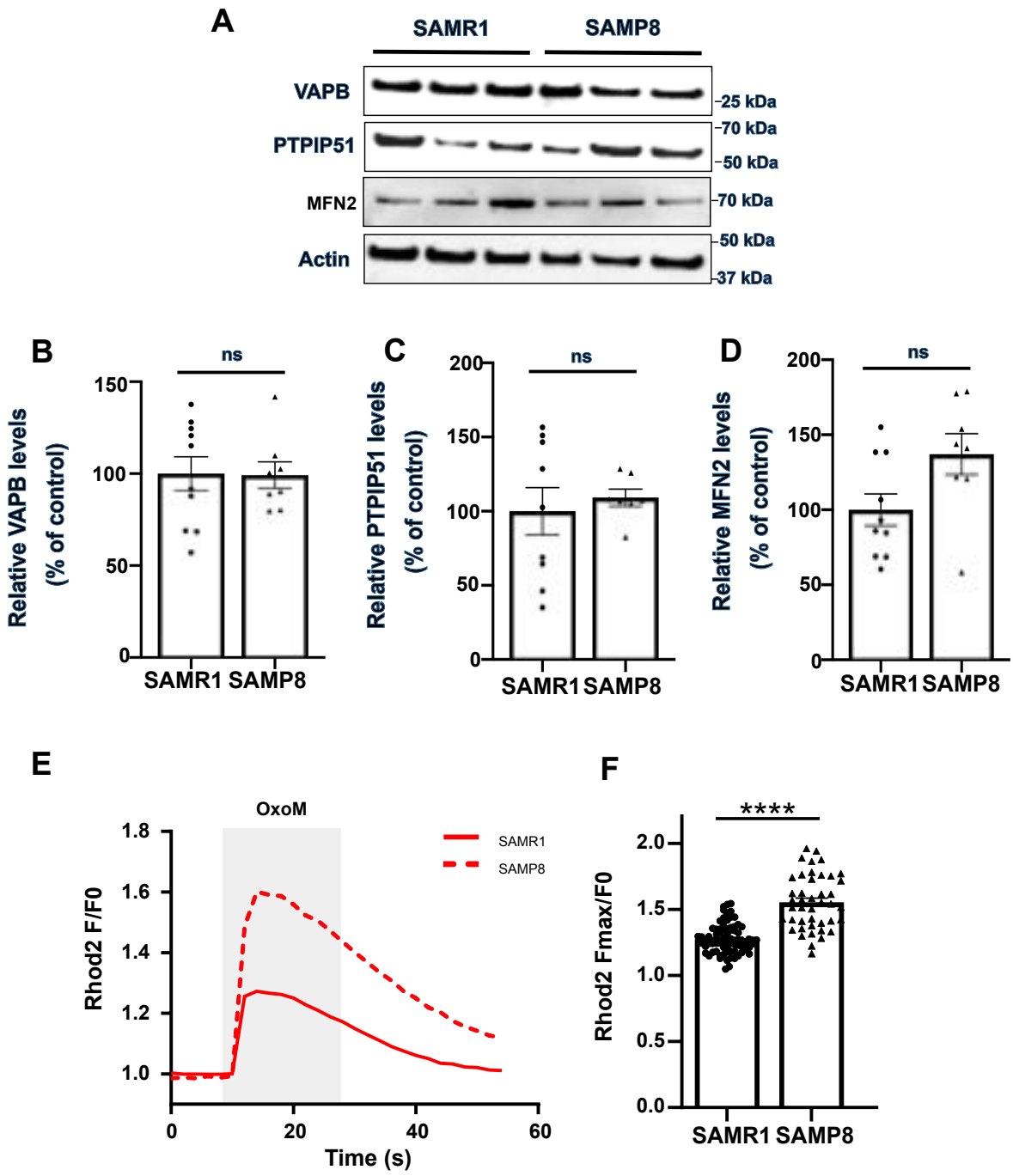
A
SAMR1
SAMP8
VAPB
PTPIP51
MFN2
Actin
25 kDa
70 kDa
50 kDa
70 kDa
50 kDa
37 kDa
B
ns
Relative VAPB levels (% of control)
150
100
50
0
SAMR1 SAMP8
C
ns
Relative PTPIP51 levels (% of control)
200
150
100
50
0
SAMR1 SAMP8
D
ns
Relative MFN2 levels (% of control)
200
150
100
50
0
SAMR1 SAMP8
E
OxoM
SAMR1
SAMP8
Rhod2 F/F0
1.8
1.6
1.4
1.2
1.0
0
20
40
60
Time (s)
F
****
Rhod2 Fmax/F0
2.0
1.5
1.0
0.5
0.0
SAMR1 SAMP8

1 C57B6

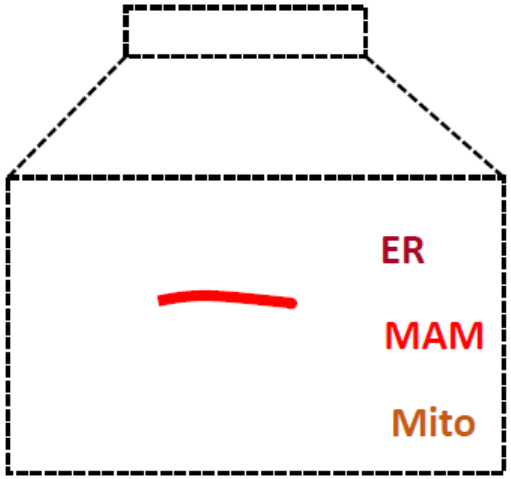

2 SAMR1

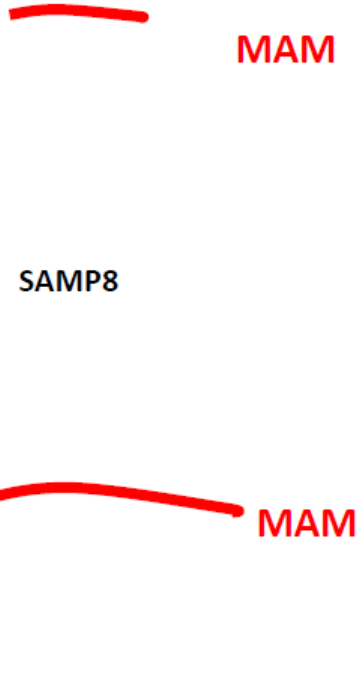

3

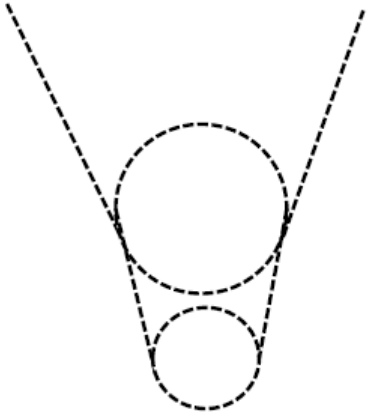

Primary culture
enteric neurons

Ca^{2+} uptake
SAMP8 vs SAMR1